Journal of Organometallic Chemistry xxx (2014) 1–7

Contents lists available at ScienceDirect

Journal of Organometallic Chemistry

journal homepage: www.elsevier.com/locate/jorganchem

Development of metal-organic framework (MOF)-B_{12} system as new bio-inspired heterogeneous catalyst

Jing Xu [a, b], Hisashi Shimakoshi [a, *], Yoshio Hisaeda [a, *]

[a] *Department of Chemistry and Biochemistry, Graduate School of Engineering, Kyushu University, Fukuoka 819-0395, Japan*
[b] *Key Laboratory of Atmospheric Environment Monitoring and Pollution Control, School of Environment Science and Technology, Nanjing University of Information Science and Technology, Nanjing 210044, China*

ARTICLE INFO

Article history:
Received 6 October 2014
Received in revised form
11 November 2014
Accepted 12 November 2014
Available online xxx

Keywords:
Metal-organic framework
Cation exchanging
B_{12}
Heterogeneous catalyst
Recycle use

ABSTRACT

A novel bimetal complex $\{Zn_4Ru_2(bpdc)_4\cdot 4C_2NH_8\cdot 9DMF\}_n$ (**1**) (H_2bpdc = 4,4′-biphenyldicarboxylic acid) was synthesized by the solvothermal method. The results of the X-ray crystallographic analysis revealed that **1** crystallizes in the orthorhombic $Pna2_1$ space group, which has a 3D 2-fold interpenetrated **hex** framework, with open channel sizes along the [010] direction of *ca.* 1.4 nm × 1.4 nm. The photosensitizer $[Ru(bpy)_3]^{2+}$ was adsorbed into the **1** to form Ru@MOF by cation exchanging. A cobalamin derivative (B_{12}), heptamethyl cobyrinate, was also effectively immobilized on Ru@MOF, and the resulting hybrid complex, B_{12}–Ru@MOF, exhibited a high reactivity for the dechlorination reaction of 1,1-bis(4-chlorophenyl)-2,2,2-trichloroethane (DDT) under an N_2 atmosphere by visible light irradiation in the solid state. The catalysis of B_{12}–Ru@MOF can still reach more than a ca. 80% conversion after third recyclings. Furthermore, the heterogeneous catalyst, B_{12}–Ru@MOF, was useful for the cobalamin-dependent reaction, such as the 1,2-migration of the acetyl group.

Introduction

The chemistry of metal-organic frameworks (MOFs) has rapidly evolved in recent years. They are a class of crystalline materials, which are constructed from well-defined molecular building blocks and metal or metal-cluster connecting nodes. Most MOF research has focused on the storage and separation of small gaseous molecules by taking advantage of their high microporosities [1–3]. However, numerous recent reports have demonstrated that active functional groups can be rationally designed and incorporated into MOFs to create hybrid materials with potential applications, including chemical sensing [4–7], catalysis [8–12], biomedical imaging [13–15], and drug delivery [16–18].

At the same time, bioorganometallic cobalamin (B_{12})-dependent enzymes catalyzes various molecular transformations that are of particular interest from the viewpoint of biological chemistry as well as synthetic organic chemistry and catalytic chemistry [19–22]. Cobalamin derivatives, such as heptamethyl cobyrinate perchlorate (Scheme 1), are used as efficient catalysts for a number of chemical transformations due to their rich redox and coordination chemistry [23,24] as well as a high nucleophilicity toward various alkyl halides in its Co(I) state [25]. The radical reactions have been widely used to synthesize complicated compounds because of the high selectivity under relatively mild conditions among the numerous synthetic methods. However, the alkyl radical formed by visible light irradiation has too short a lifetime to migrate, so it is difficult for the 1,2-migration reaction to occur using the normal B_{12} catalytic systems [26–28].

To develop the advantage of MOFs and B_{12}, we adopted the absorption method that enables immobilization of the B_{12} derivatives into the MOFs. It is expected that the pores of MOF can capture the radical to prolong its lifetime, then selectively catalyze the reaction. In this study, a porous MOF was synthesized by the solvothermal method, which can adsorb the cobalamin derivative (B_{12}) and Ru(II) photosensitizer by cation exchange, and the B_{12}–Ru@MOF hybrid was explored for the dechlorination reaction and 1,2-migration reaction in the solid state. As B_{12}–Ru@MOF works as a heterogeneous catalyst, we can separate the products and catalyst after the reaction for reuse. This is the first example of the B_{12} catalysis using the MOF system.

---

* Corresponding authors. Tel./fax: +81 92 802 2830.
E-mail addresses: shimakoshi@mail.cstm.kyushu-u.ac.jp (H. Shimakoshi), yhisatcm@mail.cstm.kyushu-u.ac.jp (Y. Hisaeda).

http://dx.doi.org/10.1016/j.jorganchem.2014.11.015

Please cite this article in press as: J. Xu, et al., Journal of Organometallic Chemistry (2014), http://dx.doi.org/10.1016/j.jorganchem.2014.11.015

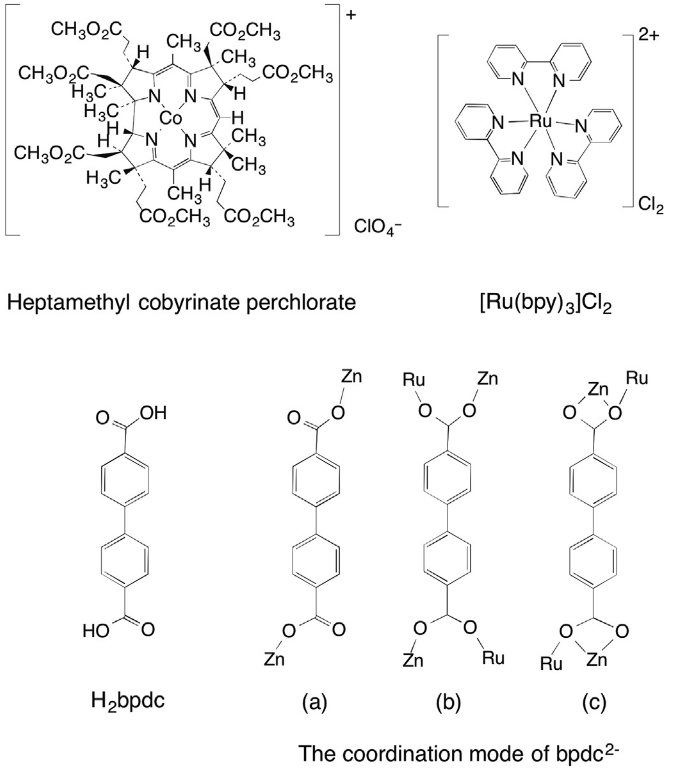

Scheme 1.

Results and discussion

Description of crystal structures

Complex $\{Zn_4Ru_2(bpdc)_4 \cdot 4C_2NH_8 \cdot 9DMF\}_n$ (**1**). The results of the X-ray diffraction analysis revealed that **1** crystallizes in the orthorhombic form with the space group of $Pna2_1$ and the asymmetric unit has a Ru(II) atom, two Zn(II) atoms, four 4,4′-biphenyldicarboxylate ligands ($bpdc^{2-}$), four $C_2NH_8^+$ (protonated dimethyl amine) molecules decomposed by the DMF solvent and nine DMF molecules. The $bpdc^{2-}$ ligands have three coordination modes (Scheme 1). Every Ru(II) center with an octahedral coordination geometry is six-coordinated by six oxygen atoms from six different $bpdc^{2-}$ ligands (four (b) and two (c) coordinated modes). Crystal view of **1** is shown in Fig. 1. The schematic drawings of **1** based on the crystal structure are also shown in Fig. 2. And as shown in Fig. 1a, two Zn(II) atoms are five-coordinated with a distorted trigonal bipyramid coordination geometry by five oxygen atoms from four different $bpdc^{2-}$ ligands (one (a), two (b) and one (c) coordinated modes). The Ru–O and Zn–O bond lengths are in the range of 2.049(1)–2.109(9) Å and 1.909(1)–1.970(1) Å, respectively as listed in Table 2.

By carefully observing the structure, the connections of the central Zn–Ru–Zn and linear linker of the $bpdc^{2-}$ ligand make the complex have a 3D framework with large channels as illustrated in Fig. 1b. Each Zn–Ru–Zn unit acts as an 8-connecting node, and the topology can be described as **hex** net with the short Schläfli symbols of $(3^6.4^{18}.5^3.6)$ [29,30]. There is a large void in the single net of the complex as mentioned above, the open channel sizes along the [010] direction are *ca.* 1.4 nm × 1.4 nm (Fig. 1b), and according to the famous Aristotle's observation that “nature abhors a vacuum”, interpenetration inevitably occurred. We found that there were two individual 3D **hex** nets interpenetrating due to the large void in the single net (Fig. 1d). It is noteworthy that there is still free space (Fig. 1c) which was calculated by the PLATON [31] analysis of 49.3% (3992.4 $Å^3$ per unit) filled by DMF molecules and its decomposed product ($C_2NH_8^+$).

Stability and gas sorption property of complex 1

Stability information about the porous structure is required and the results of the TGA analysis not only indicate the thermal stability of the MOF, but also turn out to be decisive data to ensure an optimized temperature of activation to remove the guest molecules. For complex **1**, the TGA data revealed a steady weight loss between about 50 and 250 °C, which correspond to the loss of the solvent DMF molecules (calcd. 20.38%, found 20.45%) and $C_2NH_8^+$ cations (calcd. 5.71%, found 5.85%). No weight loss then occurred until approximately 330 °C, when the entire structure starts to decompose as shown in Fig. 3. According to the TGA results, the framework **1** is stable even up to 330 °C. Before the gas adsorption tests, the activation for removing the guest molecules from the pores by heating in a vacuum is a required pre-treatment and the as-synthesized crystal samples were heated at the optimized temperature of 100 °C for 20 h. The adsorption isotherm for **1** is shown in Fig. 3 inset, in which complex **1** shows a comparatively high adsorption amount of CO_2 at 195 K and 1 atm. (40.13 $cm^3\ g^{-1}$ at STP) corresponding to 1 CO_2 molecule per formula unit. The CO_2 uptake is nearly 4 times higher than that of N_2 at 77 K (9.17 $cm^3\ g^{-1}$ at STP). The Langmuir and BET surface areas estimated from the CO_2 adsorption isotherm are 119.73 and 85.64 $m^2\ g^{-1}$, respectively. The high affinity for CO_2 of **1** may be due to the unsaturated metal sites in **1** associated with the pore structure as revealed in other MOF materials [32,33]. Thus, complex **1** may have a potential application in the separation of CO_2/N_2 mixtures and it is possible to adsorb other molecules in the cavity or on the surface of its framework.

Preparation and characterization of Ru@MOF and B_{12}–Ru@MOF

We used the MOF as a supporter to immobilize $[Ru(II)(bpy)_3]Cl_2$ and B_{12} complexes (Scheme 1) by a cation exchange reaction. This cation or anion exchange of MOFs is useful method for functionalizing MOFs [34–42]. First, we tried to absorb $[Ru(II)(bpy)_3]Cl_2$ to form Ru@MOF. The color of the $[Ru(II)(bpy)_3]Cl_2$ ethanol solution disappeared by stirring with MOF **1**, and the UV–vis spectra of the solution proved the adsorption of $[Ru(II)(bpy)_3]^{2+}$ in the cavity of the MOF (Fig. 4). The IR spectra showed that the surface of the Ru@MOFs is the same as MOF though the two samples have different colors (Fig. S1). It was calculated from the ICP-MS data that molar ratio of Ru/MOF is 3:1. The cation exchange efficiency of Ru photosensitizer considered as $\{[Ru(bpy)_3]Cl\}^+$ form is estimated as 75% in Ru@MOF.

Next, it is very important to adsorb the B_{12} complex in order to construct the B_{12}–Ru@MOF as a catalysis system. We used a heptamethyl cobyrinate perchlorate for the B_{12} complex (Scheme 1). The UV–vis spectra illustrated that the heptamethyl cobyrinate was adsorbed by Ru@MOF (Fig. 5). The evidence for the adsorption of the B_{12} complex onto Ru@MOF was obtained by an ESR analysis, and the well-defined Co(II) low spin signal typical for heptamethyl cobyrinate was observed as shown in Fig. 6 [43]. The amount of B_{12} molecules was also calculated from the ICP-MS analysis of which the molar ratio of B_{12}/MOF is 1:15. Given the size of the B_{12} and the cavity size of Ru@MOF, the number of adsorbed B_{12} molecules were smaller than that of $[Ru(bpy)_3]^{2+}$. Actually, when we first adsorbed B_{12} complex in the MOF, the obtained B_{12}-MOF did not adsorb $[Ru(bpy)_3]^{2+}$. Thus, it is likely that B_{12} complex is existed around the surface of MOF, whereas small $[Ru(bpy)_3]^{2+}$ is existed in cavity

Please cite this article in press as: J. Xu, et al., Journal of Organometallic Chemistry (2014), http://dx.doi.org/10.1016/j.jorganchem.2014.11.015

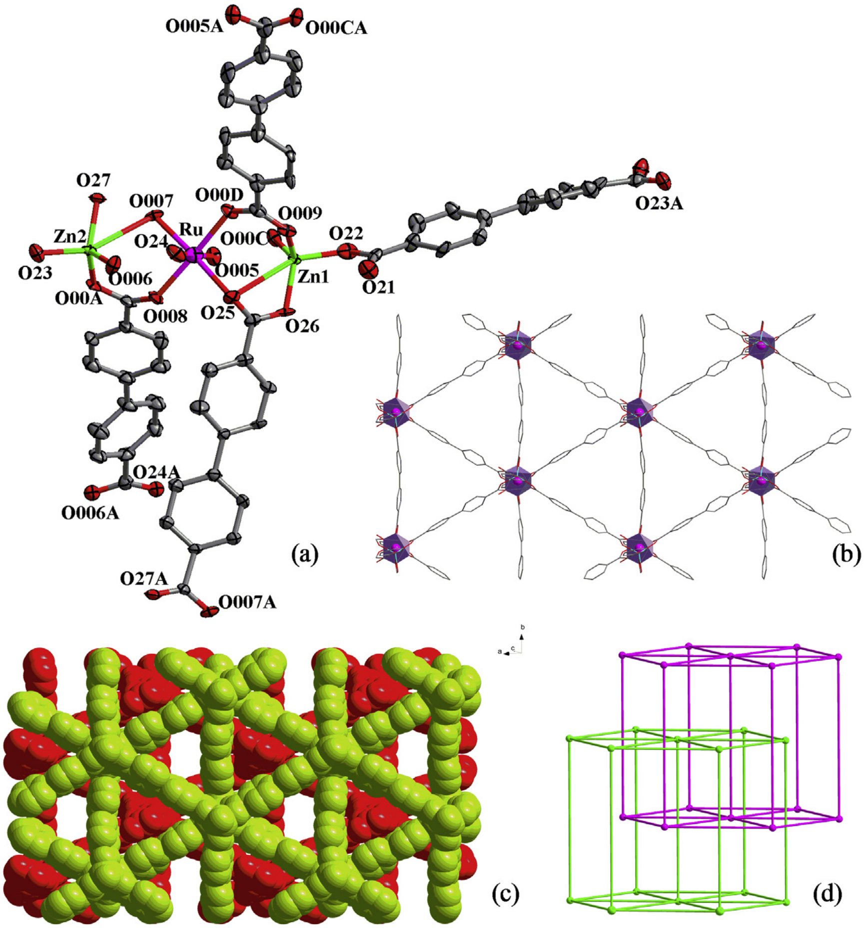

Fig. 1. (a) Coordination environment of Zn1, Zn2 and Ru in **1** with the ellipsoids drawn at the 50% probability level, and hydrogen atoms were omitted for clarity. (b) A single 3D framework from the c axis and polyhedron presentations of Zn–Ru–Zn metals. (c) The space filling mode of 2-fold interpenetrating structure. (d) Topological representation of the 2-fold interpenetrating **hex** network of **1**.

of MOF in B_{12}–Ru@MOF. In this way, the order of adsorbed molecular is important for synthesis of B_{12}–Ru@MOF.

Catalytic process of B_{12}–Ru@MOF system

The dechlorination of DDT was carried out as shown in Table 3. As DDT was irradiated with visible light in the presence of B_{12}–Ru@MOF for 4 h, the DDT was almost decomposed to form 1,1-bis(4-chlorophenyl)-2,2-dichloroethane (DDD) as the major product (Eq. (1)). The dechlorination reaction did not proceed in the dark as shown by entry 2 in Table 3. In this system, excess of triethanolamine was used as sacrificial reductant for photosensitizer recovery during the catalytic reaction. Moreover, B_{12}–Ru@MOF can be recovered by filtration and subsequently reused several times and maintain its catalytic efficiency as shown by entries 3 and 4 in Table 3.

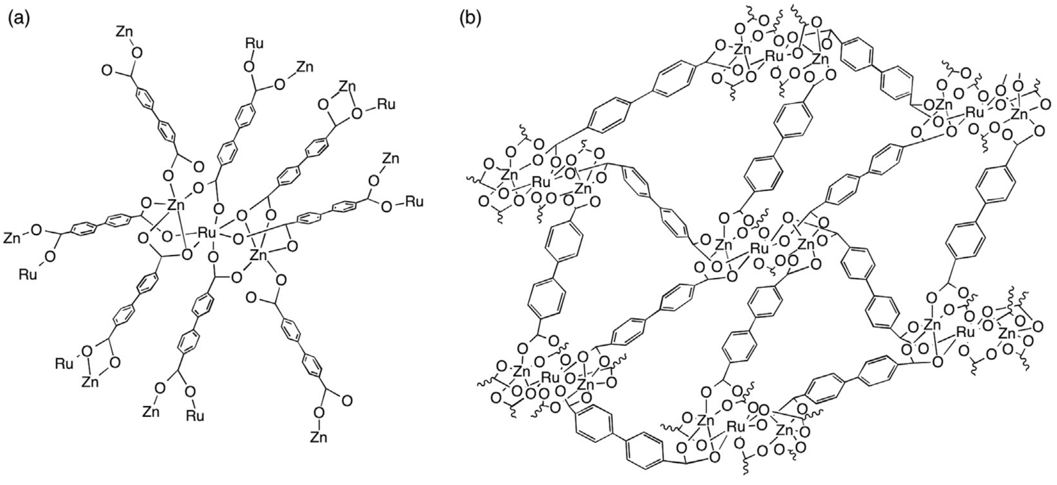

Fig. 2. (a) Zn–Ru–Zn unit structure of **1**. (b) Schematic drawing of **1** based on crystal structure.

Please cite this article in press as: J. Xu, et al., Journal of Organometallic Chemistry (2014), http://dx.doi.org/10.1016/j.jorganchem.2014.11.015

Table 1
Crystallographic data for **1**.

Chemical formula	$C_{147}H_{159}N_{13}O_{41}Ru_2Zn_4$
M	3227.48
Crystal system	Orthorhombic
Space group	$Pna2_1$
a, Å	24.572(6)
b, Å	14.514(4)
c, Å	22.314(5)
β, °	90
V, Å^3	7958(3)
Z	2
T, K	93
μ (MoKα), cm^{-1}	8.57
D_{calcd}, g cm^{-3}	1.347
λ, Å	0.71073
R_{int}	0.0992
$R_1[I > 2\sigma(I)]$[a]	0.1213
$wR_2[I > 2\sigma(I)]$[b]	0.3152

[a] $R_1 = \sum||F_o| - |F_c||/\sum|F_o|$.

[b] $wR_2 = \left|\sum w(|F_o|^2 - |F_c|^2)\right|/\sum\left|w(F_o)^2\right|^{1/2}$, where $w = 1/[\sigma^2(F_o^2) + (aP)^2 + bP]$, $P = (F_o^2 + 2F_c^2)/3$.

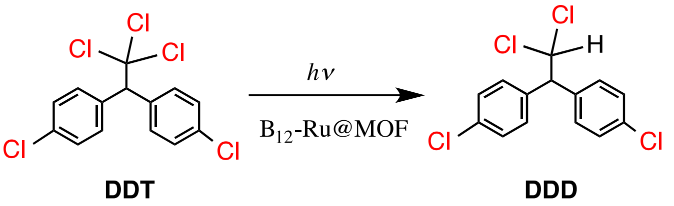

(1)

A reaction mechanism is proposed as follows: The Co(II) complex is reduced to the Co(I) species by the photosensitizer in the cavity of MOF by visible light irradiation, and the alkylated complex may be formed by the reaction of the Co(I) with DDT. The Co–C bond of the alkylated complex should be subsequently cleaved by photolysis to form the substrate radical and Co(II) species. The substrate radical will abstract H to form DDD [43].

The catalytic reaction was also carried out using 2-acetyl-1-bromo-2-ethoxycarbonylpropane as a substrate (Eq. (2)). After a 24-h reaction by visible light irradiation, conversion of the substrate reached 82% and the acetyl migrated product was formed as the main product in 68% yield as shown by entry 1 in Table 4. When EtOH was used as the reaction solvent, conversion of the substrate

Table 2
Selected bond lengths [Å] and angles [°] for **1**.

1[a]			
O(005)–Ru(02)#1	2.064(9)	O(006)–Zn(03)#2	1.909(10)
O(008)–Ru(02)#3	2.080(9)	O(009)–Zn(01)	1.949(7)
O(22)–Zn(01)#4	1.920(7)	O(23)–Zn(03)	1.954(7)
O(24)–Ru(02)	2.049(10)	O(25)–Ru(02)#5	2.109(9)
O(26)–Zn(01)#5	1.947(10)	O(27)–Zn(03)	1.970(11)
O(00)#1–Zn(03)	1.935(10)	O(00)#3–Zn(01)#1	1.927(10)
O(00)#4–Ru(02)	2.077(9)	Ru(02)–O(007)#2	2.094(9)
O(24)–Ru(02)–O(005)#6	177.7(4)	O(24)–Ru(02)–O(00)#4	85.3(4)
O(005)#6–Ru(02)–O(00)#4	92.9(4)	O(24)–Ru(02)–O(008)#2	91.7(4)
O(005)#6–Ru(02)–O(008)#2	90.1(4)	O(00)#4–Ru(02)–O(008)#2	176.7(4)
O(24)–Ru(02)–O(007)#2	94.6(4)	O(005)#6–Ru(02)–O(007)#2	86.8(4)
O(00)#4–Ru(02)–O(007)#2	87.9(4)	O(008)#2–Ru(02)–O(007)#2	91.0(4)
O(24)–Ru(02)–O(25)#7	85.9(4)	O(005)#6–Ru(02)–O(25)#7	92.8(4)
O(00)#4–Ru(02)–O(25)#7	95.3(4)	O(007)#2–Ru(02)–O(25)#7	176.9(4)
O(22)#8–Zn(01)–O(009)	104.6(4)	O(22)#8–Zn(01)–O(26)#7	107.6(5)
O(006)#3–Zn(03)–O(00)#1	114.4(5)	O(26)#7–Zn(01)–O(009)	119.5(4)
O(00)#1–Zn(03)–O(23)	108.7(4)	O(006)#3–Zn(03)–O(23)	95.6(4)
O(00)#1–Zn(03)–O(27)	113.7(4)	O(006)#3–Zn(03)–O(27)	115.5(5)
O(23)–Zn(03)–O(27)	106.9(5)		

[a] Symmetry transformations used to generate equivalent atoms:#1: $x + 1/2, -y + 2/5, z$,#2: $x - 1/2, -y + 3/2, z$,#3: $x + 1/2, -y + 3/2, z$,#4: $x + 1/2, -y + 3/2, z + 1$,#5: $x + 1/2, -y + 1/2, z$,#6: $x - 1/2, -y + 5/2, z$,#7: $x - 1/2, -y + 1/2, z$,#8: $x - 1/2, -y + 3/2, z - 1$.

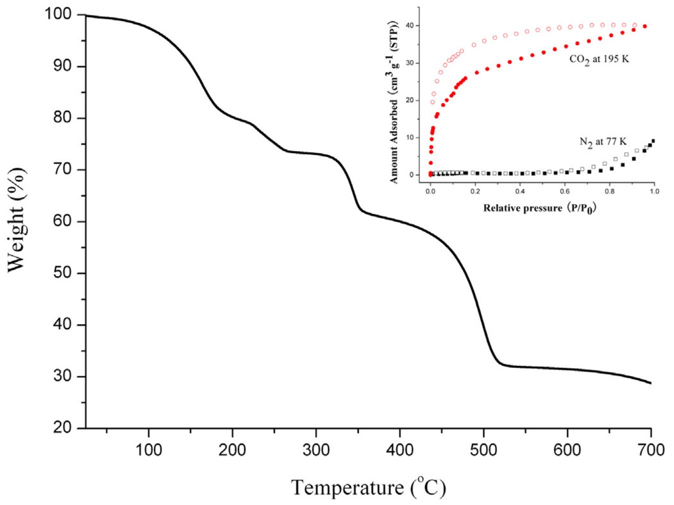

Fig. 3. TGA curves of complex **1**, inset graph is gas adsorption isotherms (CO_2 and N_2) of **1** (filled symbols: adsorption; open symbols: desorption).

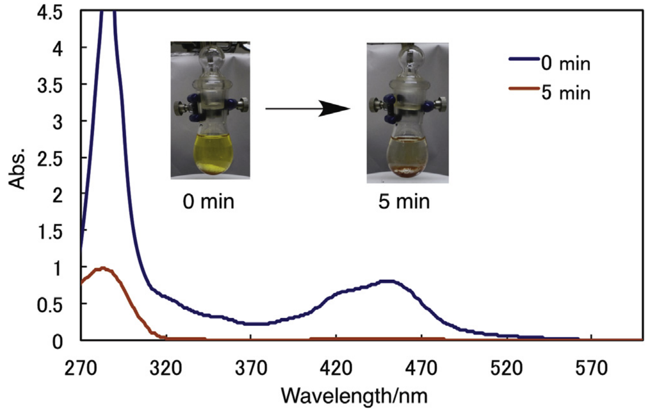

Fig. 4. UV–vis spectral change of $[Ru(bpy)_3]Cl_2$ ethanol solution in the presence of MOF **1**.

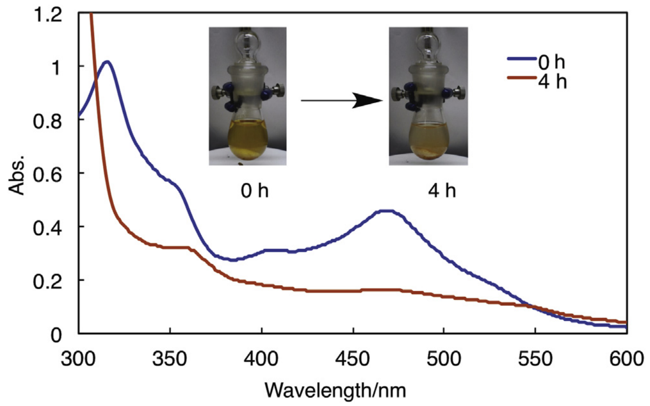

Fig. 5. UV–vis spectral change of heptametyl cobyrinate perchlorate ethanol solution in the presence of Ru@MOF.

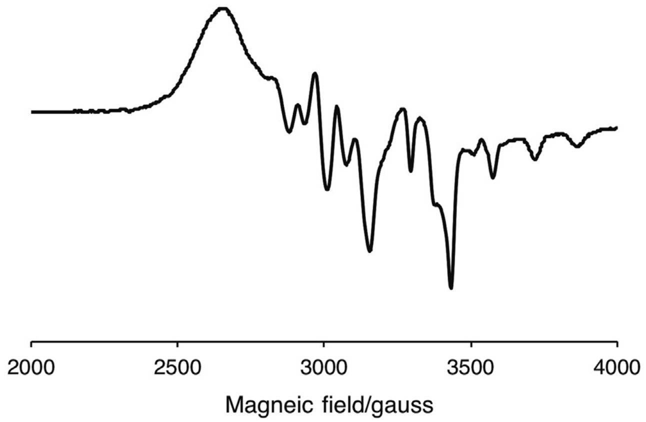

Fig. 6. ESR spectra for B_{12}–Ru@MOF at 100 K under N_2.

was only 45% and the yield of the acetyl migrated product decreased to 22% with formation of a simply reduced product (entry 2 in Table 4) since the charge neutral Co(I) state of B_{12} formed in the catalytic cycle should be dissolved in ethanol and some amount of B_{12} should be desorbed from the MOF during the stirring process. Actually, the reaction did not proceed without B_{12} using Ru@MOF as the catalyst (entry 3 in Table 4). Furthermore, the 1,2-mirgration did not proceed in the dark in which the photosensitizer can't work (entry 4 in Table 4). When we used B_{12} and $Ru(bpy)_3Cl_2$ in the absence of MOF, the conversion of the substrate is lower and the main product is the simple reduced product as shown by entry 5 in Table 4. Therefore, it is deduced that the immobilization of both the B_{12} and Ru photosensitizer in the MOF should facilitate photo-induced electron transfer from the Ru photosensitizer to B_{12} and can enhance the 1,2-migration reaction.

Table 4
1, 2-Migration reaction of acetyl group catalyzed by B_{12}–Ru@MOF system[a].

Entry	Catalyst	Solvent	Conversion[b] (%)	Products yield[c]	
				Acetyl-migrated product	Reduced product
1	B_{12}–Ru@MOF	Et_2O	82	68	13
2	B_{12}–Ru@MOF	EtOH	45	22	17
3	Ru@MOF	Et_2O	–	–	–
4[d]	B_{12}–Ru@MOF	Et_2O	–	–	–
5[e]	B_{12}, Ru	EtOH	54	7	35

[a] 1,2-Migration reactions were carried out in 5 mL of solvent under N_2 atmosphere with irradiation by a 200 W tungsten lamp ($\lambda \geq 420$ nm) for 24 h. Initial concentration: catalyst, 20 mg; substrate, 0.05 mmol; triethanolamine, 0.5 mmol.
[b] Conversion was determined by the recovery of substrate.
[c] Products were analyzed by GC–MS.
[d] The reaction was carried out in the dark.
[e] Heptamethyl cobyrinate perchlorate and $[Ru(bpy)_3]Cl_2$ were used.

Based on these results, we proposed the reaction mechanism shown in Fig. 7. The Co(II) complex is reduced to Co(I) by electron transfer from the $[Ru(bpy)_3]^{2+}$ photosensitizer, and the supernucleophilic Co(I) species reacts with the substrate to form an alkylated cobalt complex. Visible light irradiation should induce a cleavage of the carbon–cobalt bond of the alkylated cobalt complex to generate an alkyl radical intermediate **A** and Co(II) species [28,44]. The hydrogen radical abstraction from the solvent may produce the simple reduced product. While the channel of MOF can prolong the lifetime of the radical intermediate **A**, it had enough time convert to the acetyl migrated radical **B**. The radical **B** may abstract a hydrogen radical to form the acetyl migrated product.

Conclusion

A new bimetal MOF was synthesized by the solvothermal method, which has a 3D 2-fold interpenetrated **hex** topology. The framework of complex **1** has a high stability and showed a gas adsorption property. Furthermore, the cationic $[Ru(bpy)_3]^{2+}$ and B_{12} are easy to immobilize into the MOF by cation exchange reactions. The B_{12}–Ru@MOF hybrid material worked as a heterogeneous catalyst for the dechlorination and 1,2-migration reactions in the solid state and was recycled for the catalytic reaction. This is the first example of B_{12} catalysis using the MOF system, and research is now in progress on further applications of the MOF system involving bioorganometallic B_{12} reactions.

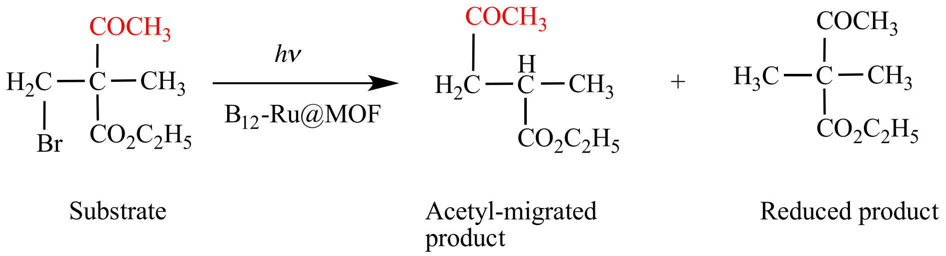

(2)

Table 3
Dechlorination of DDT catalyzed by B_{12}–Ru@MOF system[a].

Entry	Recycle	Conversion[b] (%)	Products yield[c]
			DDD
1	1st	100	99
2[d]	1st	–	–
3	2nd	89	77[e]
4	3rd	76	63[e]

[a] Dechlorination were carried out in 5 mL of Et_2O under N_2 atmosphere with irradiation by a 200 W tungsten lamp ($\lambda \geq 420$ nm) for 4 h. Initial concentration: catalyst, 20 mg; substrate, 0.05 mmol; triethanolamine, 2.5 mmol.
[b] Conversion was determined by the recovery of substrate.
[c] Products were analyzed by ^{1}H NMR.
[d] The reaction was carried out in the dark.
[e] Small amount of other dechlorinated products such as 1,1′-(2,2-dichloroethenylidene) bis(4-chlorobenzene) (DDE) and 1,1-bis(4-chlorophenyl)-2-chloroethane (DDMS) were formed.

Experimental section

Reagents and apparatus

All chemicals were obtained from commercial sources and were of GR/AR grade. 2-Acetyl-1-bromo-2-ethoxycarbonylpropane was

Please cite this article in press as: J. Xu, et al., Journal of Organometallic Chemistry (2014), http://dx.doi.org/10.1016/j.jorganchem.2014.11.015

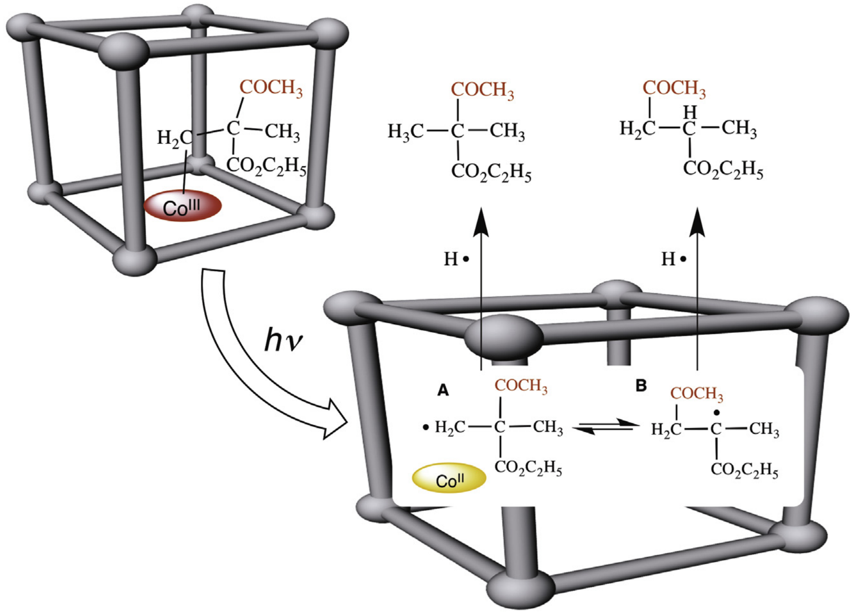

Fig. 7. Proposed catalytic mechanism for B_{12}–Ru@MOF.

synthesized by a literature method [44]. The heptamethyl cobyrinate perchlorate was also synthesized by a literature method [45,46]. The IR spectra (KBr pellets) were recorded by a JASCO FT/IR-460 Plus KH spectrometer. Elemental analyses for C, H and N were obtained from the Service Center of Elementary Analysis of Organic Compounds at Kyushu University. The UV–vis absorption spectra were recorded by a Hitachi U-3310 spectrophotometer. The ^{1}H NMR spectra were recorded by a Bruker Avance 500 spectrometer. The GC–MS were obtained using a Shimadzu GC-QP5050A equipped with a J&W Scientific DB-1 column (length 30 m; ID 0.25 mm, film 0.25 μm). The ESR spectra were obtained using a Bruker EMX-Plus X-band spectrometer at 100 K under N_2. The thermogravimetric analyses (TGA) were performed using a TGA Hitachi TG/DTA 7300 instrument heating from room temperature to 750 °C under N_2 at the heating rate of 20 °C/min. Gas sorption experiments were carried out using a Belsorp-max volumetric gas sorption instrument. Samples were outgassed under a high vacuum (less than 10^{-5} Torr) at 100 °C for 20 h, and the sample was weighed before and after the degassing procedure to confirm the complete evacuation of the solvents. ICP-MS analyses were obtained using an Agilent Technologies Agilent 7500C.

*Synthesis of complex **1** (MOF)*

The MOF $\{Zn_4Ru_2(bpdc)_4\cdot 4C_2NH_8\cdot 9DMF\}_n$ was prepared by the addition of 2.0 mg (0.004 mmol) of $Ru(bpy)_2Cl_2$, 21.0 mg (0.09 mmol) of 4,4′-biphenyldicarboxylic acid (H_2bpdc) and 11.8 mg (0.04 mmol) of $Zn(NO_3)_2\cdot 6H_2O$ in a solvent mixture of 0.45 mL DMF with 10 μL AcOH under solvothermal conditions. Dark red crystals were obtained at 100 °C after 6 days with a yield of 36%. Anal. Calcd. for $C_{147}H_{159}N_{13}O_{41}Ru_2Zn_4$ (**1**): C, 54.82%; H, 4.85%; N, 5.66%. Found: C, 54.24%; H, 4.78%; N, 5.82%. IR (KBr pellet, cm^{-1}): 3069 (ms), 1660 (s), 1606 (s), 1541 (s), 1387 (s), 1177 (ms), 1005 (ms), 847 (s), 770 (s), 703 (ms), 681 (m) (Fig. S1).

Crystal structure determination

The crystallographic data of **1** were collected at 93 K by a Bruker APEX II ULTRA CCD system equipped with graphite-monochromated MoKα radiation (λ = 0.71073 Å) and a 2 kW rotating anode generator. The data frames were integrated using SAINT (Version 6.45) [47] and merged to give a unique data set for the structure determination. Empirical absorption corrections by SADABS [48] were carried out. The structure was solved by a direct method and refined by a full-matrix least-squares technique on all *F*2 data using the SHELX suite of programs [49]. Non-hydrogen atoms were refined with anisotropic displacement factors. The details of the crystal parameters, data collection and refinements for **1** are summarized in Table 1. Selected bond lengths and angles for **1** are listed in Table 2.

Synthesis of Ru@MOF

Ru@MOF is prepared by mixing the complex **1** (MOF) (100 mg) with the EtOH solution of $[Ru(bpy)_3]Cl_2$ (75 mg) and stirring for 5 h, then washing several times with EtOH to give a apricot solid. The amount of $[Ru(bpy)_3]^{2+}$ in the MOF was determined by ICP-MS as 0.09 mmol/100 mg MOF. IR (KBr pellet, cm^{-1}): 3072 (ms), 1684 (s), 1606 (s), 1541 (s), 1423 (ms), 1394 (s), 1179 (ms), 1005 (ms), 847 (s), 770 (s), 703 (ms), 679 (m) (Fig. S1).

Synthesis of B_{12}–Ru@MOF

B_{12}–Ru@MOF was prepared by mixing the Ru@MOF (200 mg) with the EtOH solution of B_{12} (heptamethyl cobyrinate perchlorate) (10 mg) and stirring for 5 h, then washing several times with EtOH to give a brown solid. The amounts of B_{12} and $[Ru(bpy)_3]^{2+}$ were determined by ICP-MS as 2.8×10^{-3} mmol and 0.126 mmol/200 mg MOF, respectively. IR (KBr pellet, cm^{-1}): 3415 (ms), 1606 (s), 1538 (s), 1393 (s), 1005 (ms), 855 (s), 771 (s), 681 (m) (Fig. S1).

General procedure of catalytic photoreaction

A typical example of the photoreaction catalyzed by B_{12}–Ru@MOF is shown below. In the presence of a sacrificial reagent (triethanolamine), 20 mg of the catalyst and 0.05 mmol substrate in 5 mL of diethyl ether were stirred in a N_2 atmosphere with irradiation by a 200 W tungsten lamp through a cut-off filter ($\lambda \geq 420$ nm). After the photoreaction, the product was extracted by diethyl ether and hexane, then washed by water for several times.

Please cite this article in press as: J. Xu, et al., Journal of Organometallic Chemistry (2014), http://dx.doi.org/10.1016/j.jorganchem.2014.11.015

The organic layer was analyzed by GC–MS using diphenyl as the internal standard. For the dechlorination of DDT, the product was analyzed and quantified by a ^{1}H NMR measurement using 1,4-dioxane as the internal standard. The recovered catalyst was washed with Et_2O, dried under vacuum, then reused again.

Acknowledgments

This study was partially supported by the Global COE Program “Science for Future Molecular Systems” from the Ministry of Education, Culture, Sports, Science and Technology (MEXT) of Japan, and a Grant-in-Aid for Challenging Exploratory Research (No. 24655134) and a Grant-in-Aid for Scientific Research (C) (No. 23550125) from the Japan Society for the Promotion of Science (JSPS), and the 2014 Tokuyama Science Foundation.

Appendix A. Supplementary material

CCDC 1024277 contains the supplementary crystallographic data for this paper. These data can be obtained free of charge from The Cambridge Crystallographic Data Centre via www.ccdc.cam.ac.uk/data_request/cif.

Appendix B. Supplementary data

Supplementary data related to this article can be found at http://dx.doi.org/10.1016/j.jorganchem.2014.11.015.

References

[1] H.X. Deng, S. Grunder, K.E. Cordova, C. Valente, H. Furukawa, M. Hmadeh, F. Gándara, A.C. Whalley, Z. Liu, S. Asahina, H. Kazumori, M. O'Keeffe, O. Terasaki, J.F. Stoddart, O.M. Yaghi, Science 336 (2012) 1018–1023.
[2] M.M. Deshmukh, M. Ohba, S. Kitagawa, S. Sakaki, J. Am. Chem. Soc. 135 (2013) 4840–4849.
[3] N. Yanai, T. Uemura, M. Inoue, R. Matsuda, T. Fukushima, M. Tsujimoto, S. Isoda, S. Kitagawa, J. Am. Chem. Soc. 134 (2012) 4501–4504.
[4] M.D. Allendorf, R.J. Houk, L. Andruszkiewicz, A.A. Talin, J. Pikarsky, A. Choudhury, K.A. Gall, P.J. Hesketh, J. Am. Chem. Soc. 130 (2008) 14404–14405.
[5] A. Lan, K. Li, H. Wu, D.H. Olson, T.J. Emge, W. Ki, M. Hong, J.E. Li, Angew. Chem. Int. Ed. Engl. 48 (2009) 2334–2338.
[6] Z. Xie, L. Ma, K.E. deKrafft, A. Jin, W. Lin, J. Am. Chem. Soc. 131 (2009) 922–923.
[7] G. Lu, J.T. Hupp, J. Am. Chem. Soc. 132 (2010) 7832–7833.
[8] C. Wang, M. Zheng, W.B. Lin, J. Phys. Chem. Lett. 2 (2011) 1701–1709.
[9] J.M. Falkowski, T. Sawano, T. Zhang, G. Tsun, Y. Chen, J.V. Lockard, W.B. Lin, J. Am. Chem. Soc. 136 (2014) 5213–5216.
[10] L. Ma, J.M. Falkowski, C. Abney, W. Lin, Nat. Chem. 2 (2010) 838–846.
[11] L.C. Li, R. Matsuda, I. Tanaka, H. Sato, P. Kanoo, H.J. Jeon, M.L. Foo, A. Wakamiya, Y. Murata, S. Kitagawa, J. Am. Chem. Soc. 136 (2014) 7543–7546.
[12] J.L. Wang, C. Wang, W.B. Lin, ACS Catal. 2 (2012) 2630–2640.
[13] K.E. deKrafft, Z. Xie, G. Cao, S. Tran, L. Ma, O.Z. Zhou, W. Lin, Angew. Chem. Int. Ed. Engl. 48 (2009) 9901–9904.
[14] R.J. Della, W. Lin, Eur. J. Inorg. Chem. 24 (2010) 3725–3734.
[15] D. Liu, R.C. Huxford, W. Lin, Angew. Chem. Int. Ed. Engl. 50 (2011) 3696–3700.
[16] W.J. Rieter, K.M. Pott, K.M. Taylor, W. Lin, J. Am. Chem. Soc. 130 (2008) 11584–11585.
[17] W. Lin, W.J. Rieter, K.M. Taylor, Angew. Chem. Int. Ed. Engl. 48 (2009) 650–658.
[18] C. Wang, D.M. Liu, W.B. Lin, J. Am. Chem. Soc. 135 (2013) 13222–13234.
[19] K. ó Proinsias, M. Giedyk, D. Gryko, Chem. Soc. Rev. 42 (2013) 6606–6619.
[20] K. Gruber, B. Puffer, B. Kräutler, Chem. Soc. Rev. 40 (2011) 4346–4363.
[21] W. Buckel, B.T. Golding, Annu. Rev. Microbiol. 60 (2006) 27–49.
[22] K.L. Brown, Chem. Rev. 105 (2005) 2075–2149.
[23] M.A. Jabbar, H. Shimakoshi, Y. Hisaeda, Chem. Commun. (2007) 1653–1655.
[24] H. Shimakoshi, M. Tokunaga, Y. Hisaeda, Dalton Trans. (2004) 878–882.
[25] Y. Hisaeda, H. Shimakoshi, in: K.M. Kadish, K.M. Smith, R. Guilard (Eds.), In Handbook of Porphyrin Science, vol. 10, World Scientific, 2010, pp. 313–370.
[26] Y. Murakami, Y. Hisaeda, A. Ogawa, T. Ohno, J. Chem. Soc. Perkin Trans. 2 (1995) 189–191.
[27] Y. Murakami, Y. Hisaeda, X.M. Song, T. Ohno, J. Chem. Soc. Perkin Trans. 2 (1992) 1527–1528.
[28] Y. Murakami, Y. Hisaeda, J. Kikuchi, T. Ohno, M. Suzuki, Y. Matsuda, T. Matsuura, J. Chem. Soc. Perkin Trans. 2 (1988) 1237–1246.
[29] The Reticular Chemistry Structure Resource at the website of O'Keeffe group (http://rcsr.anu.edu.au/).
[30] A.F. Well, Three-dimensional Nets and Polyhedra, Wiley-Inter-Science, New York, 1977.
[31] A.L. Spek, PLATON, a Multipurpose Crystallographic Tool, Utrecht University, Utrecht, The Netherlands, 2003.
[32] A.X. Zhu, J.B. Lin, J.P. Zhang, X.M. Chen, Inorg. Chem. 48 (2009) 3882–3889.
[33] B. Mu, F. Li, K.S. Walton, Chem. Commun. (2009) 2493–2495.
[34] O.M. Yaghi, H. Li, J. Am. Chem. Soc. 117 (1995) 10401–10402.
[35] S.R. Halper, L. Do, J.R. Stork, S.M. Cohen, J. Am. Chem. Soc. 128 (2006) 15255–15268.
[36] F. Nouar, J. Eckert, J.F. Eubank, P. Forster, M. Eddaoudi, J. Am. Chem. Soc. 131 (2009) 2864–2870.
[37] J. An, N.L. Rosi, J. Am. Chem. Soc. 132 (2010) 5578–5579.
[38] E.Q. Procopio, F. Linares, C. Montoro, V. Colombo, A. Maspero, E. Barea, J.A.R. Navarro, Angew. Chem. Int. Ed. 49 (2010) 7308–7311.
[39] S. Yang, G.S.B. Martin, J.J. Titman, A.J. Blake, D.R. Allan, N.R. Champness, M. Schröder, Inorg. Chem. 50 (2011) 9374–9384.
[40] M. Kim, J.F. Cahill, H.H. Fei, K.A. Prather, S.M. Cohen, J. Am. Chem. Soc. 134 (2012) 18082–18088.
[41] M. Sadakiyo, H. Kasai, K. Kato, M. Takata, M. Yamauchi, J. Am. Chem. Soc. 136 (2014) 1702–1705.
[42] T.K. Maji, R. Matsuda, S. Kitagawa, Nat. Mater. 6 (2014) 142–148.
[43] H. Shimakoshi, L. Li, M. Nishi, Y. Hisaeda, Chem. Commun. 47 (2011) 10921–10923.
[44] Y. Murakami, Y. Hisaeda, T. Ozaki, T. Tashiro, T. Ohno, Y. Tani, Y. Matsuda, Bull. Chem. Soc. Jpn. 60 (1987) 311–324.
[45] L. Werthemann, ETH Zürich (No. 4097), Dissertation, Juris Druck and Verlag, Zürich, 1968.
[46] Y. Murakami, Y. Hisaeda, A. Kajihara, Bull. Chem. Soc. Jpn. 56 (1982) 3642–3646.
[47] SAINT, Data Reduction Software, Version 6.45A, Bruker Advanced X-ray Solution, Inc., Madison,WI, 2001.
[48] G.M. Sheldrick, SADABS, University of Goettingen, Germany, 1996.
[49] G.M. Sheldrick, SHELXL97 and SHELXS97, University of Goettingen, Germany, 1997.